Capsid Assembly is Regulated by Amino Acid Residues Asparagine 47 and 48 in The VP2 Protein of Porcine Parvovirus

Jucai Wang
Henan Academy of Agricultural Sciences
Yunchao Liu
Henan Academy of Agricultural Sciences
Yumei Chen
Zhengzhou University
Teng Zhang
Henan Academy of Agricultural Sciences
Aiping Wang
Zhengzhou University
Qiang Wei
Henan Academy of Agricultural Sciences
Dongmin Liu
Henan Zhongze Biological Engineering Co., Ltd
Fangyu Wang
Henan Academy of Agricultural Sciences
Gaiping Zhang (zhanggaiping2003@163.com)
Henan Agricultural University

Research

Keywords: Porcine parvovirus, capsid assembly, 47Asn, 48Asn, VP2 macromolecular polymers

Posted Date: September 15th, 2020

DOI: https://doi.org/10.21203/rs.3.rs-72147/v1

Version of Record: A version of this preprint was published at Veterinary Microbiology on February 1st, 2021. See the published version at https://doi.org/10.1016/j.vetmic.2020.108974.

Abstract

Background: Porcine parvovirus (PPV) is a major cause of reproductive failure in swine, and has caused huge losses throughout the world. Viral protein 2 (VP2) of PPV is a major structural protein that can self-assemble into virus-like particles (VLP) with hemagglutination (HA) activity. In order to identify the essential residues involved in the mechanism of capsid assembly and to further understand the function of HA, we analyzed a series of deletion mutants and site-directed mutations within the N-terminal of VP2 in the *Escherichia coli* (*E. coli*) system.

Results: Our results showed that deletion of first 47 amino acids from the N-terminal of VP2 protein did not affect capsid assembly, and further truncation to residue 48 Asparagine (Asn, N) caused detrimental effects. Site-directed mutagenesis experiments demonstrated that residue 47Asn reduced the assembly efficiency of PPV VLP, while residue 48Asn destroyed the stability, hemagglutination, and self-assembly characteristics of the PPV VP2 protein. These findings indicated that the residues 47Asn and 48Asn are important amino acid sites to capsid assembly and HA activity. Results from Native PAGE inferred that macromolecular polymers were critical intermediates of the VP2 protein during the capsid assembly process. Site-directed mutation at 48Asn did not affect the association of monomers to form into oligomers, but destroyed the ability of oligomers to assemble into macromolecular particles, influencing both capsid assembly and HA activity.

Conclusions: These results demonstrated that PPV capsid assembly is a complex process that is regulated by amino acids 47Asn and 48Asn, which are located at the N-terminal of VP2 and closely related to the association of macromolecular particles. Our findings provide valuable information on the mechanisms of PPV capsid assembly and the possibility of chimeric VLP vaccine development by replacing as much as 47 amino acids at the N-terminal of VP2 protein.

Background

Porcine parvovirus (PPV), a member of the genus *Parvovirus*, family *Parvoviridae*, is a common pathogen associated with reproductive failure in swine [1, 2]. It is a single-stranded DNA virus, which packages its DNA into a T = 1 nonenveloped, icosahedral capsid that is 26 nm in diameter [3]. The capsid of PPV is formed by 60 copies of a mixture of viral proteins (VP) VP1, VP2, and VP3 [4]. VP1 and VP2 are generated through alternative splicing, and they share a common C-terminal region, but VP1 contains unique 150 amino acid residues at the N-terminal extension [5]. The major capsid protein, VP2, is able to self-assemble into empty capsids alone, known as virus-like particles (VLP), which is a major antigen to induce neutralizing antibodies [6]. The VP3 protein is generated from the cleavage of VP2 at approximately 25 amino acids from the N-terminal [7].

The structure of PPV capsids has been solved by using X-ray crystallography with data to 3.5 A [8]. Similar to other parvoviruses, PPV capsid subunits consists of eight anti-parallel, β-strand motifs and four large loops, which make up most of the exposed surface of the capsid [9, 10]. Protruding “spikes”

surrounding the icosahedral three-fold axes of parvovirus are related to host-receptor recognition, cell tropism, hemagglutination (HA) activity, and antigenicity [11, 12]. Amino acid residues 93, 103, or 323, located in structural regions near the three-fold “spike” of the capsid, are responsible for the host range differences between canine parvoviruses and feline panleukopenia viruses [13]. Amino acids that determine tissue tropism were found to cluster on the viral surface, such as amino acid residues 317 or 321 of VP2 in minute virus of mice (MVM), and residues 381, 386, and 436 in PPV [8, 14]. Apart from its important roles in determining tropism and host range, the capsid also contains major antigenic sites, hemagglutination sites, lack infectious virus and are inherently safer comparable to those of the native virion [15, 16]. These beneficial characteristics make PPV VLP as the best vaccine candidate, which expressed in many different systems [17–19]. Recent years, VLP attracts broad scientific interest due to their properties as versatile scaffold in nanotechnology, such as potential therapeutic agents, targeted drug delivery, novel vaccines and so on [20–23]. PPV VLP, excepting originated advantages from their particle integrity, its simple structure makes it as an ideal platform in biomedicine to study the mechanisms of capsid assembly and virus infection, as well as the development of new vaccines [24, 25].

Virus self-assembly and virion morphogenesis are regulated by different types of protein subunits, such as monomers, dimers, trimers, pentamers, or hexamers. Both the assembly and stability are protected from the formation of multiple non-covalent interactions between protein subunits [26, 27]. Trimers, as the intermediates, may exert morphogenetic control on the icosahedral parvovirus capsids during the assembly of MVM [28, 29]. In polyomavirus, pentamers of VP1, the major capsid protein, associated with VP2 and VP3 complexes within the cytoplasm were shown to be responsible for cooperative nuclear translocation [30]. Key amino acid residues or most non-covalent interactions between protein subunits, such as hydrophobic, hydrogen bonds or salt bridges, may be critical for the assembly and stability of virions [31, 32]. As intermediates and intermolecular interactions play an important role in the function of virus capsid, it is very meaningful to further study of this work. Knowledge of capsid assembly, stability, and dynamics of PPV virions is essential to understand the virus life cycle and promote the development of antiviral vaccines and antiviral agents based on inhibiting the assembly and uncoating process.

In order to identify the functional domains of the VP2 protein involved in capsid assembly and HA activity, we constructed ten deletion mutants and three site-directed mutants within the N-terminal domain of VP2 in the *Escherichia coli* (*E. coli*) system. Our results demonstrated that truncation of the N-terminal of VP2 at amino acid residue 47 did not affected VLP assembly and HA activity. Further truncation to residue 48 Asparagine (Asn, N) caused detrimental effects. Site-directed mutagenesis demonstrated that residues 47Asn-48Asn were the key amino acid sites controlling VLP assembly and HA activity. Our results also indicated that mutation of 48Asn did not affect the formation of monomers into oligomers, but prevented the assembly of oligomers into macromolecular particles, which eventually destroyed VLP formation.

Results

Expression of mutant VP2 proteins in *E. coli* cells

In order to screen the residues involved in HA and assembly features of PPV capsids, we designed and expressed a series of deletion mutants and site-directed mutants of the VP2 protein in *E. coli* (Fig. 1). First, three N-terminal deletion mutants, with 30, 50, and 100 amino acid residues of the VP2 protein removed (namely NT-Δ30aa, NT-Δ50aa, NT-Δ100aa, respectively), were constructed. Only the NT-Δ30aa protein was successfully expressed in soluble form in *E. coli* and exhibited HA activity, reaching 2^{16} *in vitro*. However, the NT-Δ50aa and NT-Δ100aa mutant proteins were insoluble, and none of them could agglutinate guinea pig erythrocytes (Table 2 and Fig. 2). Subsequently, the NT-Δ35aa, NT-Δ40aa, NT-Δ45aa, NT-Δ46aa, NT-Δ47aa, NT-Δ48aa, and NT-Δ49aa mutants were expressed as soluble forms in the supernatant of *E. coli* cells (Fig. 2). Among these soluble mutant VP2 proteins, NT-Δ30aa, NT-Δ35aa, NT-Δ40aa, NT-Δ45aa, NT-Δ46aa, and NT-Δ47aa exhibited HA activity, with the HA titers reaching 2^{16}, 2^{16}, 2^{16}, 2^{15}, 2^{16}, and 2^{10}, respectively. Both NT-Δ48aa and NT-Δ49aa did not have HA activity (Table 2), indicating that the first 47 amino acid residues were responsible for the HA activity of PPV capsids. Interestingly, both 47 and 48 amino acid residues were asparagine. Next, we then designed and constructed another three mutants, N47K, N48K, and N47KN48K, using site-directed mutagenesis, where we replaced 47Asn and/or 48Asn amino acid with lysine (Lys, K) in the VP2 protein (Fig. 1). As shown in Fig. 3a, three mutants were expressed as soluble forms. The results from the HA test showed that only the N47K mutant exhibited HA activity, with the titers of 2^{14}, and the N48K and N47KN48K mutants showed no HA activity (Fig. 3b). These results further indicated that the 47Asn and 48Asn residues are crucial amino acids that play an important role in the structure and function of PPV capsids.

Purification of mutant VP2 proteins

Five mutant VP2 proteins—NT-Δ30aa, NT-Δ47aa, NT-Δ48aa, N47K, and N48K—and the native VP2 protein were chosen for further analyses. Fractions containing native VP2 or mutant VP2 proteins were eluted with 50 mM Tris containing 150 mM NaCl and 150 mM imidazole through Ni-NTA affinity chromatography. The eluates were then monitored continuously by UV-absorption at 280 nm, and the active fractions were recovered through size-exclusion high-performance liquid chromatography (SE-HPLC). Our SDS-PAGE analysis results showed that the purity of these proteins was over 90% (Figs. 4a–4f). As shown in the chromatogram, mutant VP2 and native VP2 protein had only one main peak, whereas the N47K protein had two main peaks (Fig. 4). As compared to the native VP2 protein, the main peak of the VP2 deletion mutants was observed at about 8.5 minutes, except for NT-Δ48aa, which was observed at 7.3 minutes (Fig. 4g and Table 3). As for the two site-directed mutants, the main peak of N48K, which appeared at around 7.5 minutes, was earlier than that of N47K and native VP2 (Fig. 3h and Table 3). Moreover, the main peak of NT-Δ48aa was in accord with N48K, which was almost at 7.3 minutes—1 minute earlier than that of the native VP2 protein (Fig. 4i and Table 3). Detailed information regarding the elution times of the VP2 mutant proteins is summarized in Table 3.

Identification of key amino acid residues in assembly of PPV capsids

Self-assembly properties of mutant VP2 proteins *in vitro* were confirmed by transmission electron microscopy (TEM) and dynamic light scattering assay (DLS). Results from TEM showed that regular VLP were observed in the native VP2 protein and NT-Δ30aa, NT-Δ47aa, and N47K, but not in NT-Δ48aa and N48K (Fig. 5). NT-Δ48aa and N48K particles showed some amount of aggregation or multimeric structure with completely irregular particles, which differed morphologically from regular VLP (Figs. 5d and 5f). Consistently, results from DLS demonstrated that the native VP2 protein, NT-Δ30aa, NT-Δ47aa, and N47K self-assembled into particles in solution, with an average diameter of 25 nm, but NT-Δ48aa and N48K existed as non-uniform particle sizes, as indicated in Fig. 6 and Table 3. Additionally, we further investigated whether the N-terminal deletion and site-directed mutant proteins retained the ability to react with the conformational monoclonal antibody 10A9, which only recognizes assembled capsids. As shown in Fig. 7, NT-Δ30aa, NT-Δ47aa, N47K (peak 1), and full-length VP2 reacted with the conformational monoclonal antibody 10A9 with titers above 1:640,000, but N47K (peak 2), NT-Δ48aa, and N48K did not. These results indicated that 47Asn and 48Asn are key amino acid residues of the VP2 protein, which have a significance effect on capsid assembly.

Analysis of mutant VP2 proteins by sucrose gradient sedimentation

Sucrose gradient sedimentation was conducted to analyze the stability and aggregation states of mutant VP2 proteins. As shown in Fig. 8a, the native VP2 protein was detected mainly in fraction 14, with one peak in the 45% sucrose gradient. The NT-Δ30aa mutant behaved similarly to the native VP2 protein, and particles were observed primarily in the 45% sucrose gradient. This suggested that, similar to the full-length VP2 protein, the NT-Δ30aa protein was assembled into VLP with high stability (Fig. 8b). As compared with the full-length VP2 protein, numerous unassembled VP2 proteins in the NT-Δ47aa, NT-Δ48aa, N47K, and N48K mutants accumulated and migrated as different protein subunits within the 5–45% sucrose gradient (Figs. 8c–8f). These results implied that the 47Asn and 48Asn residues affected the stability of the VLP structure, resulting in a large amount of intermediate aggregation, which reduced assembly efficiency and VLP formation.

Native PAGE was employed to estimate and compare unassembled subunits or intermediates in native VP2 and mutant N48K protein during the VLP formation process. As shown in Fig. 9a, there were five intermediates (**a–e**) in the unpurified VP2 capsids (lane 1). The intermediate **a** was at a position of 1236 kDa, **b** at 1048 kDa, **c** at about 720 kDa (below), **d** at 480 kDa (below), and **e** at 146 kDa. Small oligomers, such as intermediates **d** and **e**, were not detected in any sucrose layer. VP2 protein commonly exists as macromolecular particles, such as intermediate **a** and **b,** in the purified assembled VLP solution (lane 14 in Fig. 9a). When amino acid residue 48 was mutated from an Asn to Lys, numerous unassembled proteins were detected in the N48K mutant, as indicated in Fig. 9b. Three new unassembled subunits in the N48K mutant, **f** at 720 kDa, **h** 480 kDa (upper), and **i** at 242 kDa, were observed, excepting two unassembled subunits **g** at about 720 kDa (below) and **j** at about 146 KDa, located in the same position with **c** and **e** intermediates in VP2 protein (Lane 1 in Fig. 9). Importantly, these five unassembled subunits of N48K accumulated and migrated as major proteins in different sucrose layers (Fig. 9b). Notably, macromolecular polymers **a** and **b** were not detected in the N48K mutant (lane 1 and 14 in Fig. 9). The

results from liquid chromatography-tandem mass spectrometry (LC-MSMS) analysis showed that these intermediates (**a–j**) were all VP2 or mutant VP2 proteins, which represented different unassembled VP2 subunits during the VLP formation process (Fig. S1). Based on the results described above, we preliminary inferred that macromolecular polymers **a (**at 1236 kDa) and **b** (at 1048 kDa) may be critical intermediates of the VP2 protein, and site-directed mutation at the 48Asn amino acid impeded aggregation of the VP2 macromolecular particles, which is an important factor that rendered the VP2 protein defective in VLP formation during the capsid assembly process.

Discussion

PPV VP2 has both antigenicity and immunogenicity and can self-assemble into VLP *in vitro*. These VLP do not contain genetic material as found in the native virion, which makes these VLP suitable for studying viral packing and assembly, vaccine design, and biological nanomaterials. In our previous study, we investigated the HA and self-assembly characteristics of full-length VP2 protein capsids *in vitro*, and VP2 VLP showed a prominent advantage in immunogenicity and immunoprotection [19, 33]. However, the mechanisms of self-assembly of PPV capsids is still unclear. In this study, we constructed a series of mutants with N-terminal deletions and site-directed mutations in the full-length VP2 protein in order to identify regions that regulated VLP formation and HA activity. Our results demonstrated that PPV capsid assembly is a complex process that is regulated by amino acids 47Asn and 48Asn, which are located at the N-terminal of VP2 and closely related to the association of macromolecular particles.

Structural proteins, as well as their critical residues, play an irreplaceable role in protein self-association and capsid assembly. Deletion of five C-terminal residues or merely glutamic acid 257 of VP3 in the infectious bursal disease virus was found to promote capsid assembly [34]. Deletion of 27 residues or less from the N-terminal of the VP2 protein in porcine circovirus type 2 resulted in a similar icosahedral shape and immunogenicity as compared with the full-length VLP [35]. Additionally, deleting up to 125 amino acid residues from the N-terminal region of the capsid protein and truncating the C-terminal of the capsid region to 601 amino acid residues in hepatitis E virus was conducive for the self-assembly of viral particles [36]. In order to locate the key domains that may impact HA activity and assembly features of PPV capsids, ten mutant VP2 proteins were expressed in an *E. coli* system. As shown in Fig. 2, mutant proteins were expressed in the supernatant of *E. coli* cells, except NT-Δ100aa and NT-Δ50aa proteins, which aggregated as inclusion bodies. However, among these soluble mutant VP2 proteins, six mutants, NT-Δ47aa, NT-Δ46aa, NT-Δ45aa, NT-Δ40aa, NT-Δ35aa, and NT-Δ30aa, had HA activity; mutants NT-Δ49aa and NT-Δ48aa did not have HA activity (Table 2). To investigate the self-assembly and biological functions of the N-terminal deletion mutants, three mutants, NT-Δ30aa, NT-Δ47aa, and NT-Δ48aa, were chosen for further study. Results from TEM and DLS analysis confirmed that typical VLP formed in the NT-Δ30aa and NT-Δ47aa mutants, with a particle size about 25 nm, but not in NT-Δ48aa (Figs. 5–6 and Table 3). Results from the indirect enzyme-linked immunosorbent assay (ELISA) showed that NT-Δ30aa, NT-Δ47aa, and VP2 were recognized by the conformational monoclonal antibody 10A9, with titers above 1:640,000. However, NT-Δ48aa was not recognized by the antibody 10A9, which only recognizes assembled VP2 capsids, implying NT-Δ48aa did not properly assemble. The results described above

suggested that when the 48Asn amino acid was removed from the VP2 protein, the protein lost the ability to hemagglutinate guinea pig erythrocytes and was unable to self-assemble into VLP, indicating that 47Asn and 48Asn are the critical residues involved in the function of HA activity and capsid assembly during the VLP formation process.

At physiological conditions, homogeneous VLP assembled, while at acidic or basic pHs, with low ionic strength, the major assemblies were small intermediates [37]. It has been reported that residues involved in hydrogen bonds, hydrophobic interactions, and salt bridges or heterologous peptide insertions may have an effect on the stability and assembly of viral proteins [25, 31, 38].Site-directed mutations in capsid protein has proved to modify the properties or function of virus capsids [39–41]. In this study, deleting the first 47 amino acid residues within the N-terminal region of the VP2 capsid protein had no significant effect on HA and self-assembly characteristics of PPV capsids. However, deletion of amino acid 48 resulted in loss of HA activity and VLP formation. Considering that amino acids 47 and 48 are both asparagine, three mutants (N47K, N48K, and N47KN48K) were designed and constructed by replacing 47Asn and/or 48Asn amino acid with lysine in the VP2 protein. As shown in Fig. 3a, the mutants were expressed as soluble proteins in *E. coli*. Results from the HA assay indicated that only the N47K mutant exhibited HA activity, with 2^{14} titers (Fig. 3b). The ability of purified N47K and N48K to self-assemble into VLP *in vitro* was assessed by TEM, DLS, and ELISA assays. Results from TEM and DLS revealed that VLP were observed in the N47K mutant, but not in the N48K mutant (Figs. 5–6). As shown in Fig. 7, the N48K mutant was not recognized by the conformational monoclonal antibody 10A9, which only reacts with assembled capsids. Site-directed mutations or deletion of amino acids within the N-terminal of the VP2 protein changed the morphology and function of PPV VLP. Sucrose gradient sedimentation was employed to analyze the effects of mutations on the formation and stability of PPV capsids during the VLP formation process. Notably, results from sucrose gradient sedimentation showed that the mutant VP2 proteins were distributed within the 5–45% sucrose, implying that there were unassembled protein subunits that accumulated, as seen in the NT-Δ47aa, NT-Δ48aa, N47K and N48K mutants, but not the NT-Δ30aa mutant and native VP2 protein (Fig. 8). This suggested that 47Asn-48Asn residues are critical amino acids involved in the self-assembly process and stability of PPV VLP. Residue 47Asn reduced the assembly efficiency of PPV VLP, while residue 48Asn destroyed the stability, hemagglutination, and self-assembly characteristics of the PPV VP2 protein. We preferred to deem that because the stability structure of PPV VLP was destroyed, and hence made VP2 capsids lost its HA activity. However, further research needs to be performed in order to better understand the underlying mechanism.

Virus capsids are assembled from stable forms or assembly intermediates. These structures may be soluble monomers or small oligomers (e.g., dimers, trimers, pentamers, hexamers), and can be detected in the dynamic balance of assembled-unassembled capsids, depending on the virus and conditions [26]. The trimer was confirmed as the transient intermediate existing during the assembly of MVM VLP, and capsid formation was dependent upon stronger intertrimer interactions that were equally spaced in an equatorial belt surrounding each trimer [28, 29]. Present studies have shown that 48Asn residue in the VP2 protein directly impacted the structure or function of viral particles, and deletion or mutation at this

site rendered the VP2 protein defective in assembling capsids. As shown in Fig. 8f, results from sucrose gradient sedimentation showed that a number of unassembled subunits existed in the N48K mutant, which might represent different oligomers or polymers formed by the VP2 protein. Native PAGE was employed to evaluate the native conditions of these unassembled subunits in the N48K mutant during the VLP formation process. Comparing the N48K mutant with the native VP2 protein, intermediates **a** (at about 1236 kDa) and **b** (at about 1048 kDa) were detected as major protein subunits in VP2 capsids, while intermediates **f** (at 720 kDa), **g** (720 kDa below), **h** (at 480 kDa upper), **i** (at 242 kDa), and **j** (at 146 kDa) aggregated in the N48K mutant (Fig. 9). These intermediates in the N48K mutant appeared as small oligomers, such as dimers (**j** at 146 kDa), trimers (**i** at 242 kDa), pentamers (**h** at 480 kDa upper), as well as a complex (**f** at 720 kDa and **g** at 720 kDa below), and accumulated in large amounts, which eventually had a significant negative affect on the formation of VLP. Importantly, the intermediates **a** and **b** were not observed in the N48K mutant, which were two important intermediates of VP2 protein during the VLP assembly process. We preliminarily deduced that the macromolecular particles, intermediate **a** located at about 1236 kDa and intermediate **b** at about 1048 kDa, may be formed by pentamers or trimers. Although the mechanisms of PPV capsid assembly remains unclear, our data suggested that site-directed mutagenesis at 48Asn did not affect the association of monomers to form into oligomers, but destroyed the ability of oligomers to assemble into macromolecular particles. This resulted in adverse effects on VLP formation and HA activity.

Conclusions

In summary, we investigated the key amino acid sites within the N-terminal region of the VP2 protein, which may control and affect VLP formation and HA activity of PPV capsids. Deletion of the first 47 amino acids within the N-terminal had no effect on VLP assembly, whereas deletion of the first 48 amino acids resulted in loss of VLP formation. Site-directed mutagenesis experiments indicated that residue 47Asn reduced the assembly efficiency of PPV VLP, while residue 48Asn had a detrimental effect on the stability and function of PPV capsids. Further research revealed that mutation at 48Asn impeded the ability of oligomers to assemble into macromolecular particles, which eventually had a negative effect on VLP formation. These findings provided new insights into understanding the mechanisms of PPV capsid assembly and valuable information regarding designing chimeric VLP vaccines by replacing the first 47 amino acid residues at the N-terminal of the VP2 protein.

Methods

Construction of capsid VP2 mutants

Ten mutants with amino acids deleted from the N-terminal region of the VP2 capsid protein and three site-directed mutations in VP2 were constructed using the *E. coli* expression system (Fig. 1). The VP2 gene was truncated at the N-terminal by inserting PCR-amplified fragments flanked by *Nde* I and *Xho* I restriction enzyme sites into the pET28a vector (Novagen, Malaysia) described previously [33], as indicated in Table 1. Recombinant vectors were confirmed by using enzyme digestion and DNA

sequencing (Sangon Biotech, Shanghai, China). Three site-directed VP2 mutants were obtained *in vitro* by using the Fast Site-Directed Mutagenesis Kit (Tiangen, Beijing, China). The pET28a plasmid, containing the full-length VP2 gene (1737 bp), was amplified by three pairs of mutation primers (Table 1). Briefly, amplification reactions were carried out in a total volume of 50 μL, containing 2 μL of template DNA, 2 μL of each forward and reverse primer (10 μM), 10 μL of 5× Fast Alteration Buffer, 1 μL of Fast Alteration DNA Polymerase (1.0 U/μL), and 33 μL of RNAse-free water. Polymerase chain reaction (PCR) procedure was followed as described below. Initial denaturation was at 2 minutes at 95°C followed by 18 cycles, each cycle consisting of 20 seconds at 94°C, 10 seconds at 55°C and 2.5 minute at 68°C. The final extension was 5 minutes at 72°C. After amplification, the PCR product was digested with *Dpn* I restriction enzyme at 37°C for 1 hour, and then 5 μL of the digestion product was transformed into FDM competent cells to screen for mutants. Desired mutants were identified by DNA sequencing.

Expression and purification of mutated VP2 protein

Full-length and mutant VP2 proteins were expressed in the *E. coli* system. Cells were grown in Luria-Bertani (LB) media supplemented with chloramphenicol 25 mg/L, kanamycin 50 mg/L, and L-Arabinose 2 g/L. Then isopropyl-β-D-thiogalactopyranoside (IPTG) was added at a final concentration of 0.15 mM to induce recombinant protein expression. After culturing the cells for 12 hours at 25°C at 200 rpm, the cells were harvested by centrifugation, resuspended in buffer A (150 mM NaCl, 50 mM Tris, pH 8.0), and lysed by ultrasonic treatment on ice. The expression of target recombinant protein was detected by western blotting (WB).

VP2 and mutant VP2 protein in the supernatant of *E. coli* cells were purified by a two-step method, using Ni-NTA affinity chromatography (Merck, Darmstadt, Germany) followed by SE-HPLC. Clarified cell lysates were pumped onto a Ni-NTA column balanced with 10 bed volumes of buffer A. After washing with 10 bed volumes of buffer B (150 mM NaCl, 50 mM Tris, 25 mM imidazole, pH 8.0), VP2 or mutant VP2 proteins were eluted with buffer C (150 mM NaCl, 50 mM Tris, 150 mM imidazole, pH 8.0). Fractions were further separated by SE-HPLC, using a Superdex™ 200 10/300 GL (GE Healthcare, Pittsburgh, PA, USA) column as described below. A Superdex™ 200 10/300 GL column was equilibrated with 10 bed volumes of buffer A at a rate of 1 mL/min. Subsequently, samples were applied to the Superdex™ 200 10/300 GL column. After binding, fractions were further eluted with buffer A. Elution fractions were collected and determined by 12% (v/v) SDS-PAGE. Fractions containing VP2 protein or mutant VP2 proteins were filtered with a 0.22 μm filter (Merck Millipore, Darmstadt, Germany) and quantified using a Micro BCA™ protein assay kit (Solarbio, Beijing, China). Importantly, all purification procedures were carried out at 4°C, and purified fractions were stored at −80°C to retain biological activity.

SDS-PAGE and western blotting analysis

SDS-PAGE and western blotting were conducted to detect protein expression as described below. First, 5× loading buffer was added to each cell lysate or fraction. Then mixtures were heated at 100°C for 10 minutes, resolved by 12% SDS-PAGE, and finally stained with Coomassie blue (Beyotime, Shanghai, China). For WB, samples were transferred from SDS-PAGE to PVDF membranes (Bio-Rad, Richmond,

California, USA). VP2 or mutant VP2 proteins were detected using a horseradish peroxidase (HRP)-conjugated anti-his monoclonal antibody (Jackson ImmunoResearch, Philadelphia, PA, USA) at a dilution of 1:5,000. Membranes were observed with enhanced chemiluminescent reagent (NCM Biotech, Suzhou, China) or 3-amino-9-ethylcarbazole solution (ZSGB-BIO, Beijing, China), and examined by light microscopy (Leica DMI3000B) (Feica Microsystems, Wetzlar, Germany).

HA analysis

Supernatants containing VP2 or mutant VP2 were diluted with PBS for standard HA assays. To perform a HA test, 50 μL of clarified cell lysates containing VP2 or mutant VP2 were 2-fold diluted with PBS in a 96-V-shaped-well microtiter plate. Then 50 μL of guinea pig erythrocytes (0.8%) were added to each well. The plate was incubated at 37°C for 1 hour. HA titers were defined as the highest dilution that completely agglutinated guinea pig erythrocytes.

Indirect enzyme-linked immunosorbent assay

An indirect enzyme-linked immunosorbent assay was carried out using the conformational antibody 10A9, which only recognizes assembled capsids, as prepared in our previous study. First, 96-well plates were coated with purified mutant VP2 proteins, wild-type VP2 protein, or pET 28a empty vector, and then blocked with 5% skim milk in PBST at 4°C at least 8 hours. The conformational antibody 10A9 was used as the primary antibody and added into 96-well plates at 37°C for 30 minutes. After washing with PBST for five times, an HRP-conjugated goat anti-mouse IgG antibody (Jackson ImmunoResearch, Philadelphia, PA, USA) was used as the secondary antibody and incubated in the plate at 37°C for 45 minutes. Finally, antibody binding was analyzed by adding TMB solution (Solarbio, Beijing, China), and 2 M H_2SO_4 was added to stop the reaction. The optical density at 450 nm was recorded using a microplate reader (Omega Bio-Tek, Inc., Norcross, GA, Germany). All the experiments were performed in triplicate.

Transmission electron microscopy analysis

Transmission electron microscopy analysis was performed using a negative-staining method. Purified proteins were stained with 2% phosphotungstic acid (Solarbio, Beijing, China) for 1 minute and air-dried for 5 minutes at room temperature after removing excessive sample with filter paper. Grids were observed and imaged using a JEM-1400 (JEOL, Tokyo, Japan) at an acceleration voltage of 100 kV, with a magnification of 120,000×.

Dynamic light scattering assay

A dynamic light scattering assay was measured at room temperature using the Nano Particle Analyzer (Malvern, Beijing, China). Samples were diluted to an identical concentration of 0.1 mg/mL before measurement, and all determinations were conducted at a scattering angle of 90° and equilibrated to 25°C. At least 20 acquisitions were collected for each sample. This assay was performed in triplicate for data analysis.

Sucrose gradient sedimentation analysis

VP2 and mutant VP2 proteins were purified in sucrose gradients. A four-step gradient of 5%, 15%, 30%, and 45% (wt/vol) sucrose was prepared in Tris-HCL buffer. All gradients were fractionated by bottom puncture, prepared in 12-mL tubes by loading 2 mL/step, and incubated at 4°C at least 8 hours to allow diffusion into a continuous gradient. Samples were firstly precipitated with 40% saturated ammonium sulfate (Sinopharm, Beijing, China), dialyzed with Tris-HCL buffer, loaded onto the gradients, and then ultracentrifuged at 200,000 ´ g in a P40ST rotor at 4°C for 36 hours (Hitachi, Ibaraki, Japan). After ultracentrifugation, samples in each fraction were electrophoresed via SDS-PAGE and identified by WB as described above. Native morphology of these samples was further examined using the NativePAGE™ Novex® Bis-Tris Gel System (Thermo Fisher Scientific, Waltham, MA, USA), and identified by LC-MSMS analysis (Sangon Biotech, Shanghai, China).

Abbreviations

Asn, N: Asparagine; DLS: dynamic light scattering assay; *E. coli*: *Escherichia coli*; ELISA: indirect enzyme-linked immunosorbent assay; HA: hemagglutination; HRP: horseradish peroxidase; LC-MSMS: liquid chromatography-tandem mass spectrometry; Lys, K: lysine; MVM: minute virus of mice; PCR: polymerase chain reaction; PPV: porcine parvovirus; SE-HPLC: size-exclusion high-performance liquid chromatography; VP: Viral proteins; VLP: virus-like particles; WB: western blotting.

Declarations

Ethics approval and consent to participate

Not applicable.

Consent for publication

Not applicable.

Availability of data and materials

All data generated or analyzed during this study are included in this published article and its supplementary information files.

Competing interests

The authors declare that they have no competing interests.

Funding

This work was supported by grants from the National Key R&D Program (2017YFD0501103) and "1125 talent gathering plan" of Zhengzhou, as well as the Special Fund for Scientific Research and Development

of Henan Academy of Agricultural Sciences ([2017]76-21).

Authors' contributions

WJC, LYC, ZT, and CYM conceived of the experiments, WJC, LYC, WAP, WQ, LDM, and WFY performed the experiments, WJC, LYC and ZGP wrote the paper. All authors read and approved the final manuscript.

Acknowledgements

Not applicable.

Authors' information

a. Henan Provincial Key Laboratory of Animal Immunology, Henan Academy of Agricultural Sciences, Zhengzhou, 450002, China. b. College of Animal Science and Veterinary Medicine, Henan Agricultural University, Zhengzhou, 450002, China. c. School of Life Sciences, Zhengzhou University, Zhengzhou, 450001, China. d. Henan Zhongze Biological Engineering Co., Ltd, Zhengzhou, China. e. Jiangsu Co-Innovation Center for the Prevention and Control of Important Animal Infectious Disease and Zoonose, Yangzhou University, Yangzhou, China

References

1. Oh WT, Kim RY, Nguyen VG, Chung HC, Park BK: Perspectives on the Evolution of Porcine Parvovirus. *Viruses* 2017, 9.
2. Song C, Zhu C, Zhang C, Cui S: Detection of porcine parvovirus using a taqman-based real-time pcr with primers and probe designed for the NS1 gene. *Virol J* 2010, 7:353.
3. Kaufmann B, Simpson AA, Rossmann MG: The structure of human parvovirus B19. *Proc Natl Acad Sci U S A* 2004, 101:11628-11633.
4. Meszaros I, Olasz F, Csagola A, Tijssen P, Zadori Z: Biology of Porcine Parvovirus (Ungulate parvovirus 1). *Viruses* 2017, 9.
5. Chandramouli S, Medina-Selby A, Coit D, Schaefer M, Spencer T, Brito LA, Zhang P, Otten G, Mandl CW, Mason PW, et al: Generation of a parvovirus B19 vaccine candidate. *Vaccine* 2013, 31:3872-3878.
6. Rueda P, Fominaya J, Langeveld JP, Bruschke C, Vela C, Casal JI: Effect of different baculovirus inactivation procedures on the integrity and immunogenicity of porcine parvovirus-like particles. *Vaccine* 2000, 19:726-734.
7. Tu M, Liu F, Chen S, Wang M, Cheng A: Role of capsid proteins in parvoviruses infection. *Virol J* 2015, 12:114.
8. Simpson AA, Hebert B, Sullivan GM, Parrish CR, Zadori Z, Tijssen P, Rossmann MG: The structure of porcine parvovirus: comparison with related viruses. *J Mol Biol* 2002, 315:1189-1198.

9. Hafenstein S, Bowman VD, Sun T, Nelson CD, Palermo LM, Chipman PR, Battisti AJ, Parrish CR, Rossmann MG: Structural comparison of different antibodies interacting with parvovirus capsids. *J Virol* 2009, 83:5556-5566.
10. Yuan W, Parrish CR: Canine parvovirus capsid assembly and differences in mammalian and insect cells. *Virology* 2001, 279:546-557.
11. Hueffer K, Parrish CR: Parvovirus host range, cell tropism and evolution. *Curr Opin Microbiol* 2003, 6:392-398.
12. Llamas-Saiz AL, Agbandje-McKenna M, Parker JS, Wahid AT, Parrish CR, Rossmann MG: Structural analysis of a mutation in canine parvovirus which controls antigenicity and host range. *Virology* 1996, 225:65-71.
13. Chang SF, Sgro JY, Parrish CR: Multiple amino acids in the capsid structure of canine parvovirus coordinately determine the canine host range and specific antigenic and hemagglutination properties. *J Virol* 1992, 66:6858-6867.
14. Agbandje-McKenna M, Llamas-Saiz AL, Wang F, Tattersall P, Rossmann MG: Functional implications of the structure of the murine parvovirus, minute virus of mice. *Structure* 1998, 6:1369-1381.
15. Antonis AF, Bruschke CJ, Rueda P, Maranga L, Casal JI, Vela C, Hilgers LA, Belt PB, Weerdmeester K, Carrondo MJ, Langeveld JP: A novel recombinant virus-like particle vaccine for prevention of porcine parvovirus-induced reproductive failure. *Vaccine* 2006, 24:5481-5490.
16. Organtini LJ, Lee H, Iketani S, Huang K, Ashley RE, Makhov AM, Conway JF, Parrish CR, Hafenstein S: Near-Atomic Resolution Structure of a Highly Neutralizing Fab Bound to Canine Parvovirus. *J Virol* 2016, 90:9733-9742.
17. Guo C, Zhong Z, Huang Y: Production and immunogenicity of VP2 protein of porcine parvovirus expressed in Pichia pastoris. *Arch Virol* 2014, 159:963-970.
18. Rymerson RT, Babiuk L, Menassa R, Vanderbeld B, Brandle JE: Immunogenicity of the capsid protein VP2 from porcine parvovirus expressed in low alkaloid transgenic tobacco. *Molecular Breeding* 2003, 11:267-276.
19. Ji P, Liu Y, Chen Y, Wang A, Jiang D, Zhao B, Wang J, Chai S, Zhou E, Zhang G: Porcine parvovirus capsid protein expressed in Escherichia coli self-assembles into virus-like particles with high immunogenicity in mice and guinea pigs. *Antiviral Res* 2017, 139:146-152.
20. Sanchez-Sanchez L, Tapia-Moreno A, Juarez-Moreno K, Patterson DP, Cadena-Nava RD, Douglas T, Vazquez-Duhalt R: Design of a VLP-nanovehicle for CYP450 enzymatic activity delivery. *J Nanobiotechnology* 2015, 13:66.
21. Lino CA, Caldeira JC, Peabody DS: Display of single-chain variable fragments on bacteriophage MS2 virus-like particles. *J Nanobiotechnology* 2017, 15:13.
22. Li X, Meng X, Wang S, Li Z, Yang L, Tu L, Diao W, Yu C, Yu Y, Yan C, Wang L: Virus-like particles of recombinant PCV2b carrying FMDV-VP1 epitopes induce both anti-PCV and anti-FMDV antibody responses. *Appl Microbiol Biotechnol* 2018, 102:10541-10550.

23. Crisci E, Barcena J, Montoya M: Virus-like particles: the new frontier of vaccines for animal viral infections. *Vet Immunol Immunopathol* 2012, 148**:**211-225.
24. Mohsen MO, Zha L, Cabral-Miranda G, Bachmann MF: Major findings and recent advances in virus-like particle (VLP)-based vaccines. *Semin Immunol* 2017, 34**:**123-132.
25. Carreira A, Menendez M, Reguera J, Almendral JM, Mateu MG: In vitro disassembly of a parvovirus capsid and effect on capsid stability of heterologous peptide insertions in surface loops. *J Biol Chem* 2004, 279**:**6517-6525.
26. Mateu MG: Assembly, stability and dynamics of virus capsids. *Arch Biochem Biophys* 2013, 531**:**65-79.
27. Reguera J, Grueso E, Carreira A, Sanchez-Martinez C, Almendral JM, Mateu MG: Functional relevance of amino acid residues involved in interactions with ordered nucleic acid in a spherical virus. *J Biol Chem* 2005, 280**:**17969-17977.
28. Riolobos L, Reguera J, Mateu MG, Almendral JM: Nuclear transport of trimeric assembly intermediates exerts a morphogenetic control on the icosahedral parvovirus capsid. *J Mol Biol* 2006, 357**:**1026-1038.
29. Perez R, Castellanos M, Rodriguez-Huete A, Mateu MG: Molecular determinants of self-association and rearrangement of a trimeric intermediate during the assembly of a parvovirus capsid. *J Mol Biol* 2011, 413**:**32-40.
30. Nelson LM, Rose RC, Moroianu J: Nuclear import strategies of high risk HPV16 L1 major capsid protein. *J Biol Chem* 2002, 277**:**23958-23964.
31. Reguera J, Carreira A, Riolobos L, Almendral JM, Mateu MG: Role of interfacial amino acid residues in assembly, stability, and conformation of a spherical virus capsid. *Proc Natl Acad Sci U S A* 2004, 101**:**2724-2729.
32. Bleker S, Sonntag F, Kleinschmidt JA: Mutational analysis of narrow pores at the fivefold symmetry axes of adeno-associated virus type 2 capsids reveals a dual role in genome packaging and activation of phospholipase A2 activity. *J Virol* 2005, 79**:**2528-2540.
33. Wang J, Liu Y, Chen Y, Wang A, Wei Q, Liu D, Zhang G: Large-scale manufacture of VP2 VLP vaccine against porcine parvovirus in Escherichia coli with high-density fermentation. *Appl Microbiol Biotechnol* 2020, 104**:**3847-3857.
34. Chevalier C, Lepault J, Da Costa B, Delmas B: The last C-terminal residue of VP3, glutamic acid 257, controls capsid assembly of infectious bursal disease virus. *J Virol* 2004, 78**:**3296-3303.
35. Mo X, Li X, Yin B, Deng J, Tian K, Yuan A: Structural roles of PCV2 capsid protein N-terminus in PCV2 particle assembly and identification of PCV2 type-specific neutralizing epitope. *PLoS Pathog* 2019, 15**:**e1007562.
36. Li TC, Takeda N, Miyamura T, Matsuura Y, Wang JC, Engvall H, Hammar L, Xing L, Cheng RH: Essential elements of the capsid protein for self-assembly into empty virus-like particles of hepatitis E virus. *J Virol* 2005, 79**:**12999-13006.

37. Sanchez-Rodriguez SP, Munch-Anguiano L, Echeverria O, Vazquez-Nin G, Mora-Pale M, Dordick JS, Bustos-Jaimes I: Human parvovirus B19 virus-like particles: In vitro assembly and stability. *Biochimie* 2012, 94**:**870-878.
38. Mateo R, Diaz A, Baranowski E, Mateu MG: Complete alanine scanning of intersubunit interfaces in a foot-and-mouth disease virus capsid reveals critical contributions of many side chains to particle stability and viral function. *J Biol Chem* 2003, 278**:**41019-41027.
39. Cotmore SF, Tattersall P: Mutations at the base of the icosahedral five-fold cylinders of minute virus of mice induce 3'-to-5' genome uncoating and critically impair entry functions. *J Virol* 2012, 86**:**69-80.
40. Joshi A, Nagashima K, Freed EO: Mutation of dileucine-like motifs in the human immunodeficiency virus type 1 capsid disrupts virus assembly, gag-gag interactions, gag-membrane binding, and virion maturation. *J Virol* 2006, 80**:**7939-7951.
41. Moyer CL, Besser ES, Nemerow GR: A Single Maturation Cleavage Site in Adenovirus Impacts Cell Entry and Capsid Assembly. *J Virol* 2016, 90**:**521-532.

Tables

Table 1
Primers Used for Construction of N-terminal Deletion or Site-directed Mutants of VP2 Protein

Number	Name	Sequence(5′-3′)	Residues sites
1	NTΔ100aa-F	ggaattccatatggcgcatacccaaatggt	101-579aa
	NTΔ100aa-R	ccgctcgagttaatacagtttccgtggaatgag	
2	NTΔ50aa-F	ggaattccatatggaatttcagtatctgggcgaag	51-579aa
	NTΔ50aa-R	ccgctcgagttaatacagtttccgtggaatgag	
3	NTΔ49aa-F	ggaattccatatgaccgaatttcagtatctggg	50-579aa
	NTΔ49aa-R	ccgctcgagttaatacagtttccgtggaatgag	
4	NTΔ48aa-F	ggaattccatatgcagaccgaatttcagtatctgg	49-579aa
	NTΔ48aa-R	ccgctcgagttaatacagtttccgtggaatgag	
5	NTΔ47aa-F	ggaattccatatgaatcagaccgaatttcagtatctg	48-579aa
	NTΔ47aa-R	ccgctcgagttaatacagtttccgtggaatgag	
6	NTΔ46aa-F	ggaattccatatgaacaatcagaccgaatttcagtat	47-579aa
	NTΔ46aa-R	ccgctcgagttaatacagtttccgtggaatgag	
7	NTΔ45aa-F	ggaattccatatgtttaacaatcagaccgaatttcagt	46-579aa
	NTΔ45aa-R	ccgctcgagttaatacagtttccgtggaatgag	
8	NTΔ40aa-F	ggaattccatatggtgtctacgggtacctttaaca	41-579aa
	NTΔ40aa-R	ccgctcgagttaatacagtttccgtggaatgag	
9	NTΔ35aa-F	ggaattccatatggcaggcggcgttg	36-579aa
	NTΔ35aa-R	ccgctcgagttaatacagtttccgtggaatgag	
10	NTΔ30aa-F	ggaattccatatgggtggcgggcgc	31-579aa
	NTΔ30aa-R	ccgctcgagttaatacagtttccgtggaatgag	
11	N47K-F	tgtctacgggtacctttaaaaatcagaccga	47aa
	N47K-R	tttaaaggtacccgtagacacgccaacgc	
12	N48K-F	ctacgggtacctttaacaaacagaccgaat	48aa
	N48K-R	tttgttaaaggtacccgtagacacgccaac	
13	N47KN48K-F	tctacgggtacctttaaaaaacagaccgaatttcagtatc	47-48aa
	N47KN48K-R	gatactgaaattcggtctgtttttttaaaggtacccgtaga	

Table 2. HA Results for Mutated VP2 Proteins

Name	HA Titers
VP2-full	2^{16}
NT-Δ100aa	None
NT-Δ50aa	None
NT-Δ49aa	None
NT-Δ48aa	None
NT-Δ47aa	2^{10}
NT-Δ46aa	2^{16}
NT-Δ45aa	2^{15}
NT-Δ40aa	2^{16}
NT-Δ35aa	2^{16}
NT-Δ30aa	2^{16}
N47K	2^{14}
N48K	None
N47KN48K	None

Table 3. Characteristics of Mutated VP2 Proteins

Name	HA Titers	SE-HPLC Time (min)	DLS Size (nm)	TEM Size (nm)	ELISA titers
VP2-full	2^{16}	8.5	25, 25, 25	~25 nm	1:1280,000
NT-Δ30aa	2^{16}	8.4	24, 24, 25	~25 nm	1:1280,000
NT-Δ47aa	2^{10}	8.6	25, 25, 26	~25 nm	1:1280,000
NT-Δ48aa	None	7.3	32, 45, 30	None	None
N47K	2^{14}	8.4	23, 24, 25	~25 nm	1:640,000 (peak1)
N48K	None	7.5	20, 37, 45	None	None

Figures

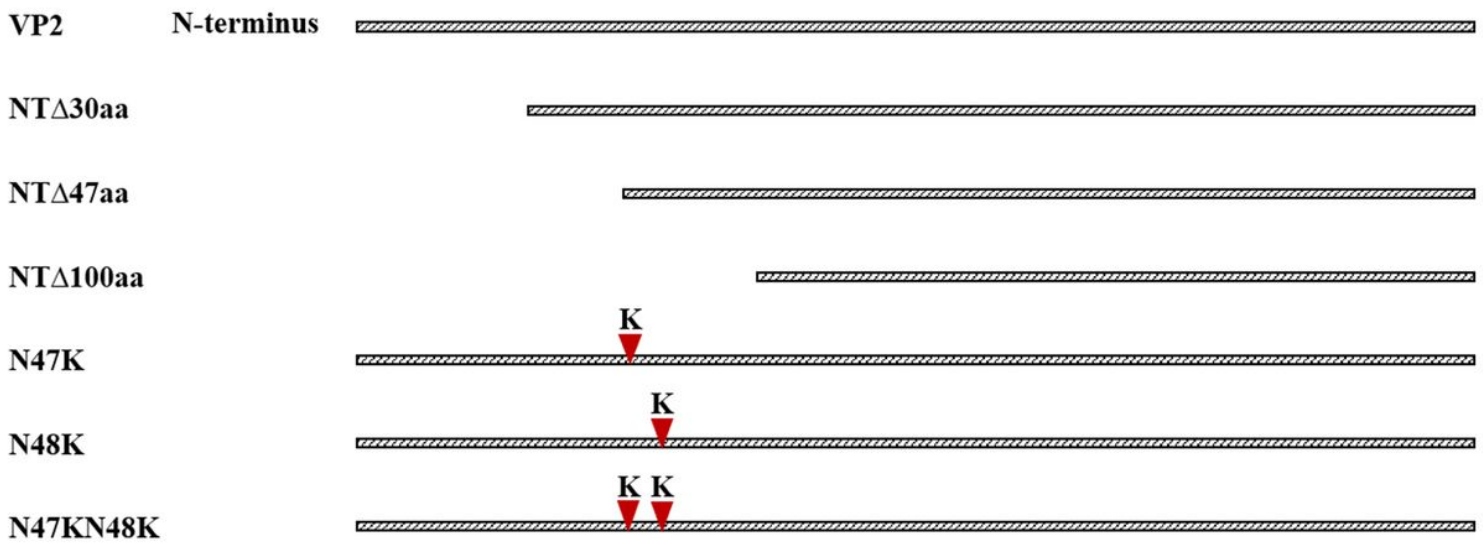

Figure 1

Diagrams of deletion mutants and site-directed mutants of VP2 protein. Ten deletion mutants (only shown three) and three site-directed mutants were constructed. Three N-terminal deletion mutants, with 30, 47, and 100 amino acid residues of the VP2 protein removed, namely NT-Δ30aa, NT-Δ50aa, NT-Δ100aa, were constructed and expressed in E. coli. Three site-directed mutants were designed and constructed by replacing 47Asn (N) and/or 48Asn (N) with a lysine (Lys, K) in the full-length VP2 protein.

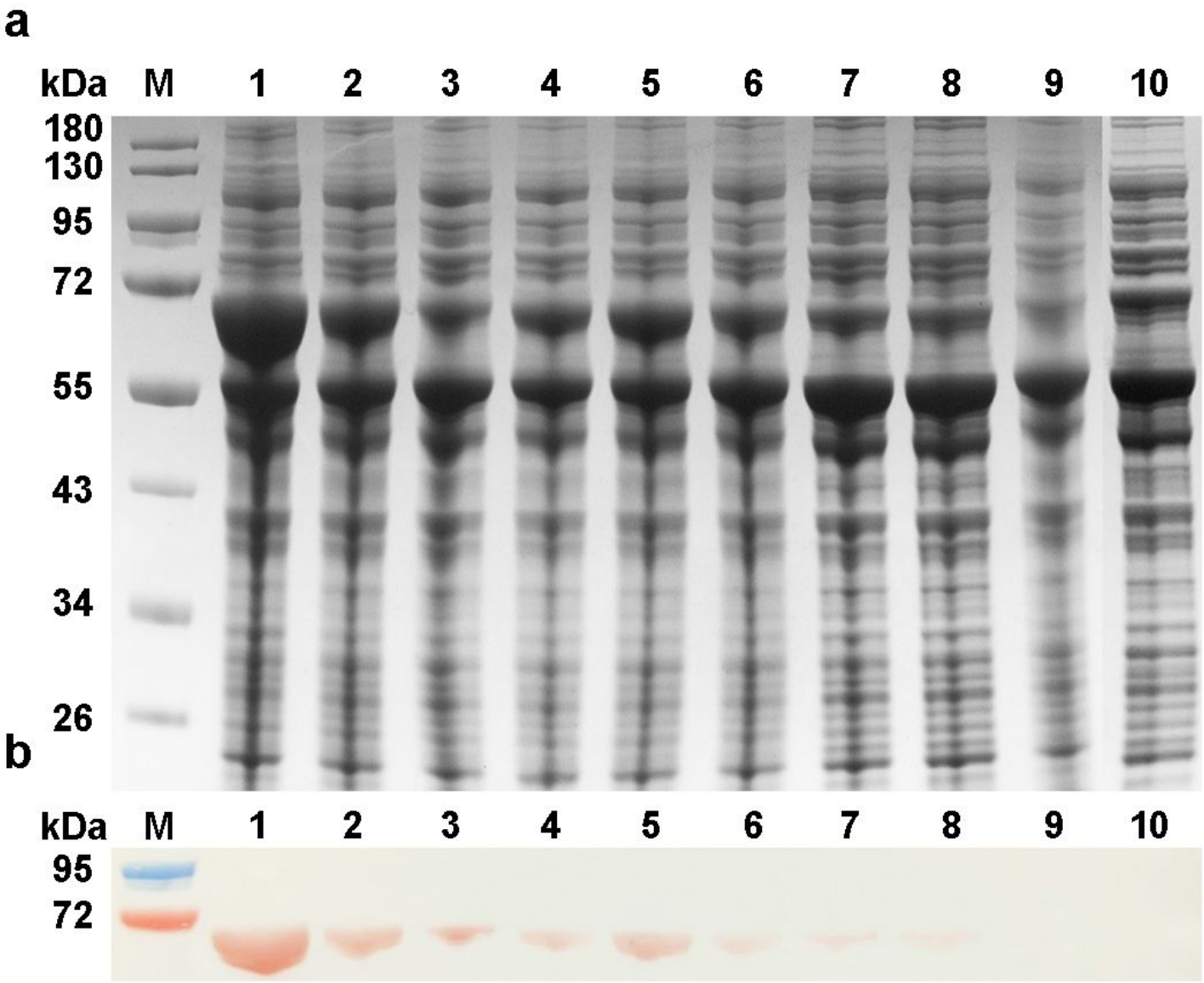

Figure 2

Expression and identification of mutants with deletions in the N-terminal region of the VP2 protein by SDS-PAGE and western blotting. a SDS-PAGE analysis of mutated VP2 proteins. b Western blotting analysis of mutated VP2 proteins with an anti-His monoclonal antibody. M, Marker; 1, NT-Δ30aa; 2, NT-Δ35aa; 3, NT-Δ40aa; 4, NT-Δ45aa; 5, NT-Δ46aa; 6, NT-Δ47aa; 7, NT-Δ48aa; 8, NT-Δ49aa;9, NT-Δ50aa; 10, NT-Δ100aa.

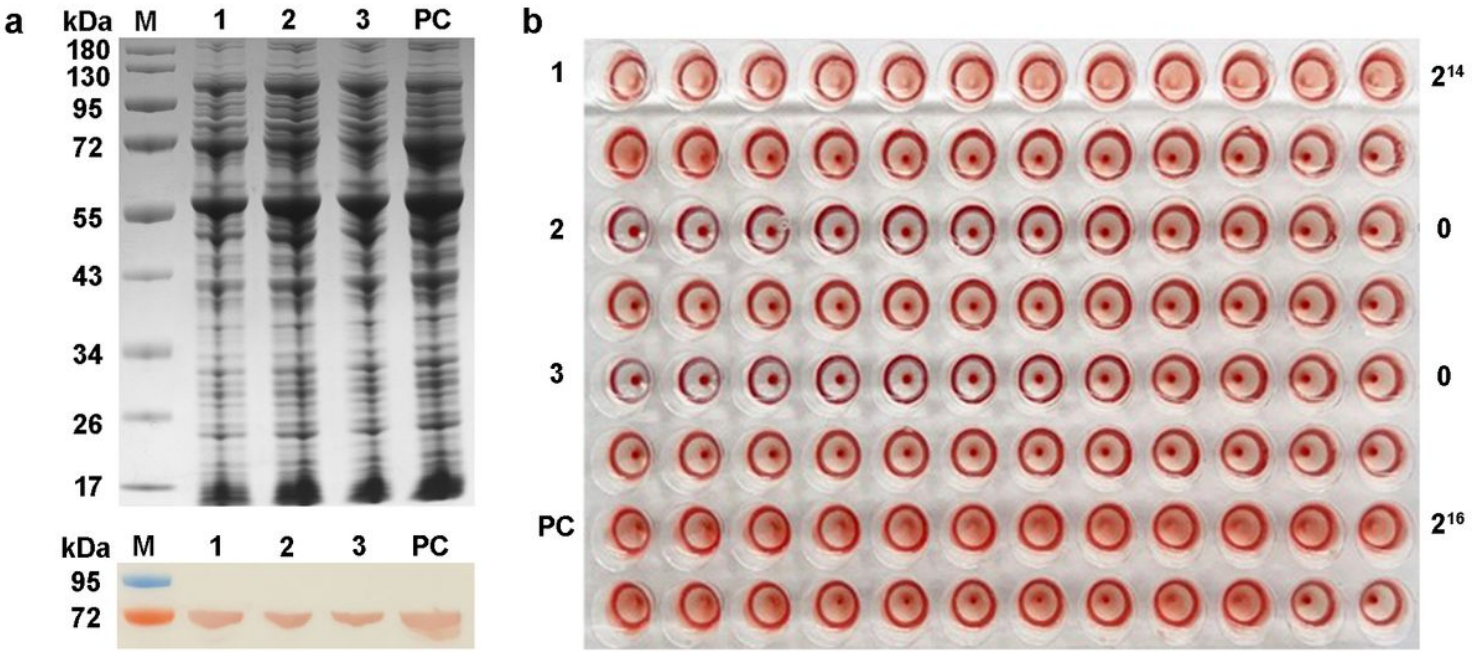

Figure 3

Identification of site-directed mutants of the VP2 protein. a Expression and identification of site-directed mutants of the VP2 protein by SDS-PAGE and western blotting. M, Marker;1, N47K; 2, N48K; 3, N47KN48K; PC, full-length VP2 protein. b HA results for site-directed mutants of VP2 protein. 1, N47K; 2, N48K; 3, N47KN48K; PC, full-length VP2 protein.

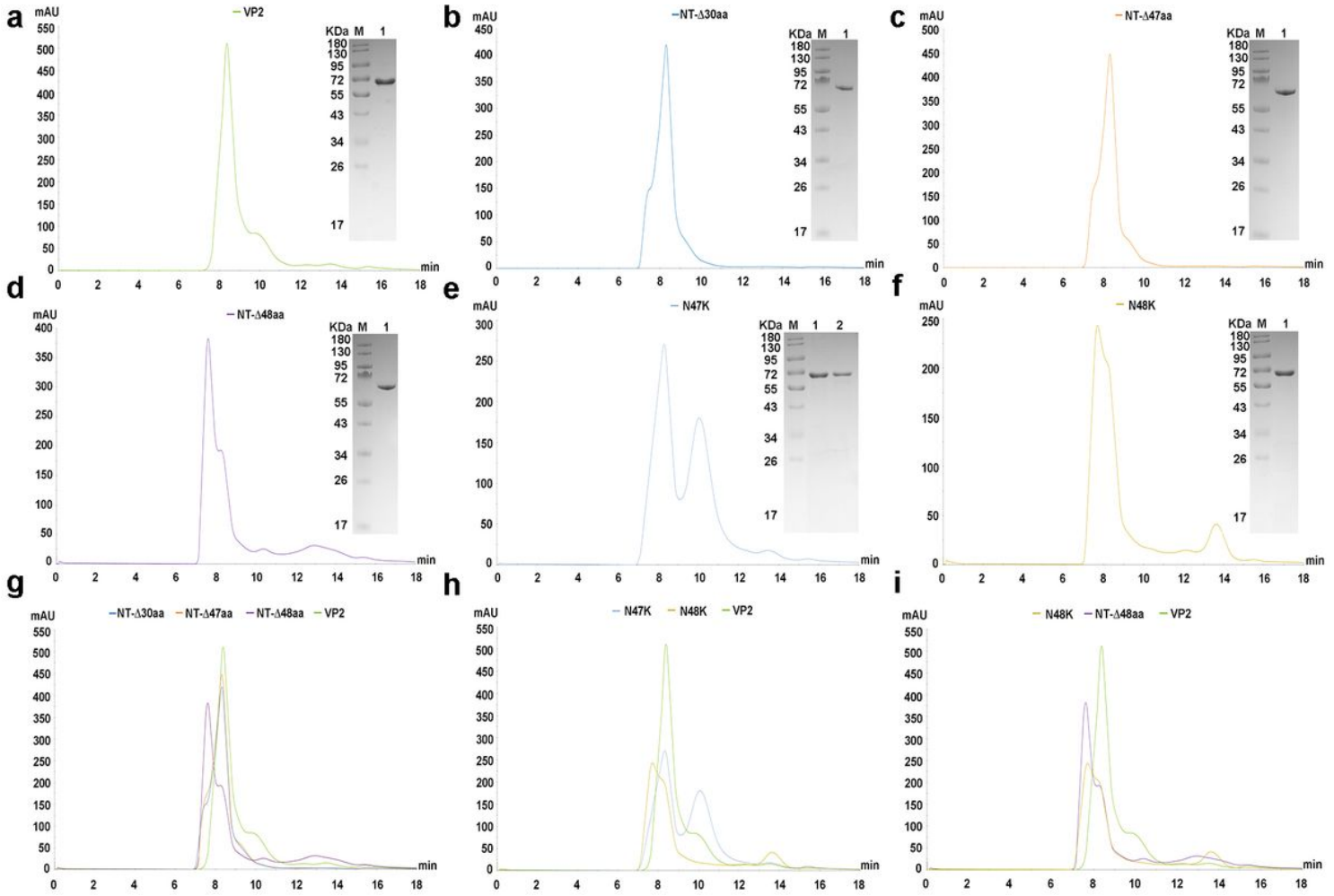

Figure 4

Protein purification results of PPV VP2 protein and mutant VP2 proteins. The purity of VP2 protein or mutant VP2 proteins was more than 90%. Eluted fractions from a Ni-NTA column were further evaluated by SE-HPLC analysis, using a Superdex™ 200 10/300 GL column. In the chromatogram, the y-axis indicates the absorbance (280 nm, mAU), while the x-axis indicates elution time (min). a VP2; b NT-Δ30aa; c NT-Δ47aa; d NT-Δ48aa; e N47K; f N48K; g results compared between NT-Δ30aa, NT-Δ47aa, and NT-Δ48aa with full-length VP2; h results compared between N47K and N48K with full-length VP2 protein; i results compared between N48K and NT-Δ48aa with full-length VP2.

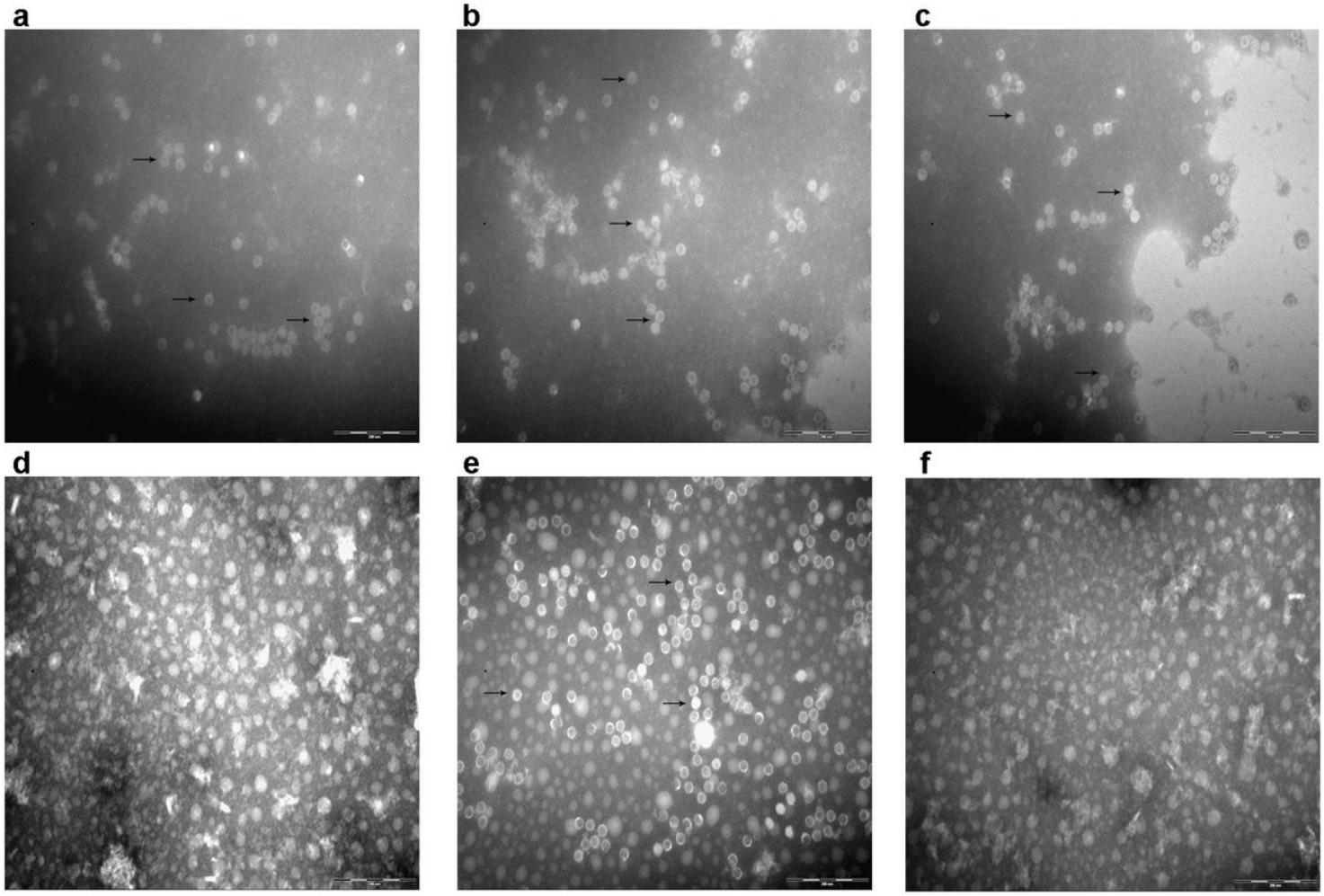

Figure 5

Transmission electron microscopy results of purified mutant VP2 proteins. a VP2; b NT-Δ30aa; c NT-Δ47aa; d NT-Δ48aa; e N47K; f N48K. The bar was 200 nm, and VLP are indicated with arrows.

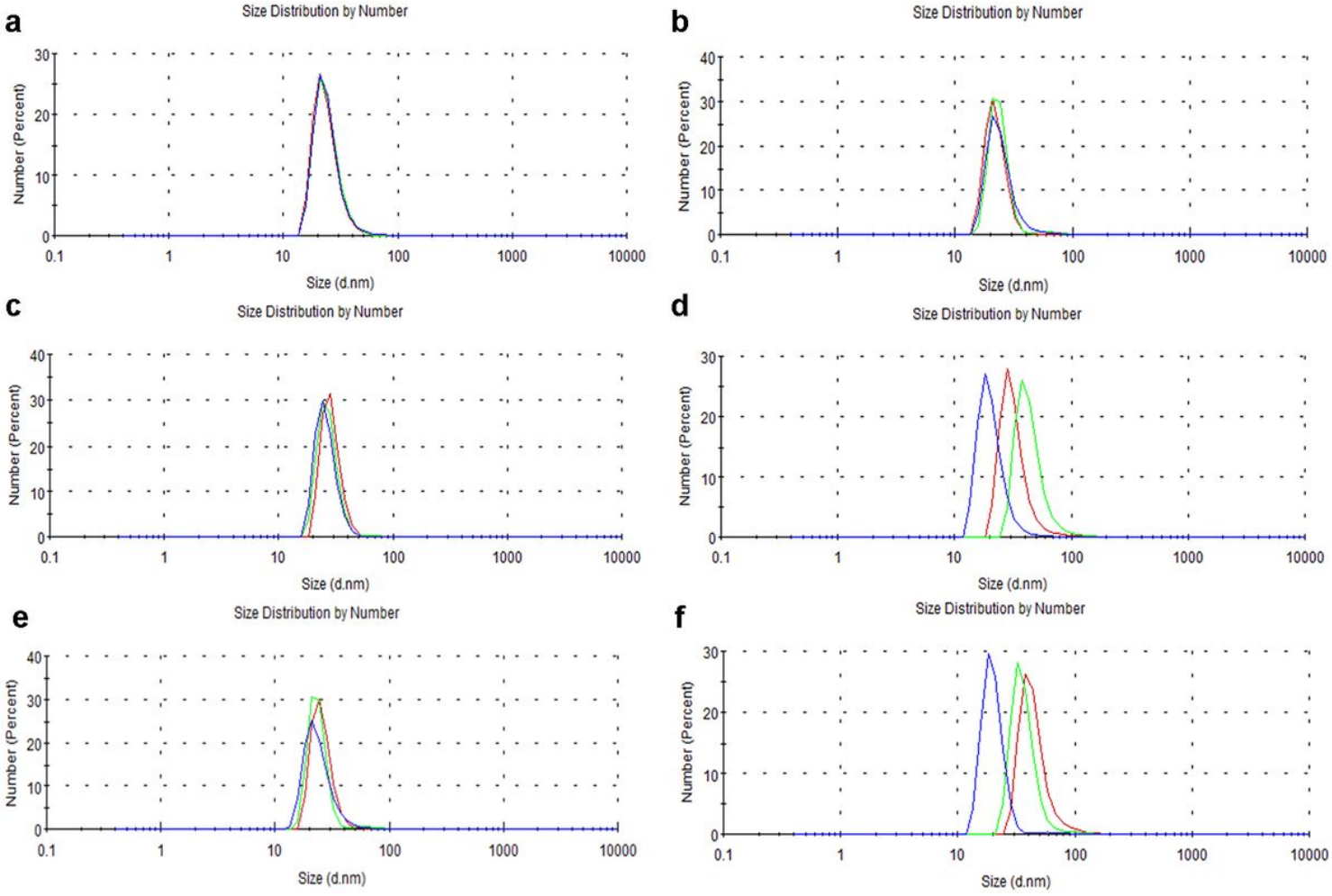

Figure 6

Dynamic light scattering results of mutant VP2 proteins. a VP2; b NT-Δ30aa; c NT-Δ47aa; d NT-Δ48aa; e N47K; f N48K. At least 20 acquisitions were collected from each sample. Each sample was performed in triplicate for data analysis.

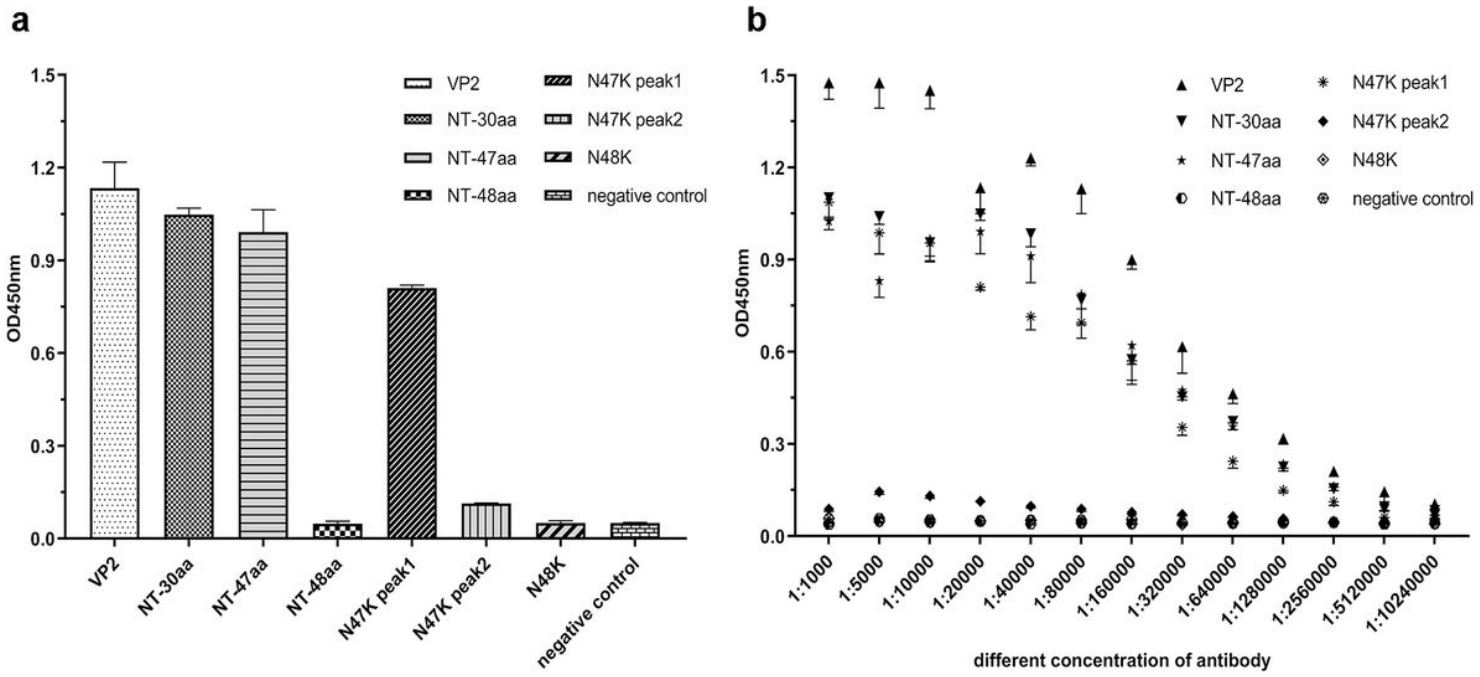

Figure 7

Binding characteristics of purified mutant VP2 proteins using the conformational antibody 10A9. a ELISA results for mutant VP2 proteins using the antibody 10A9 at a certain concentration. Antibody 10A9 was diluted 1:20,000. b Antibody titers of mutant VP2 proteins using the antibody 10A9.

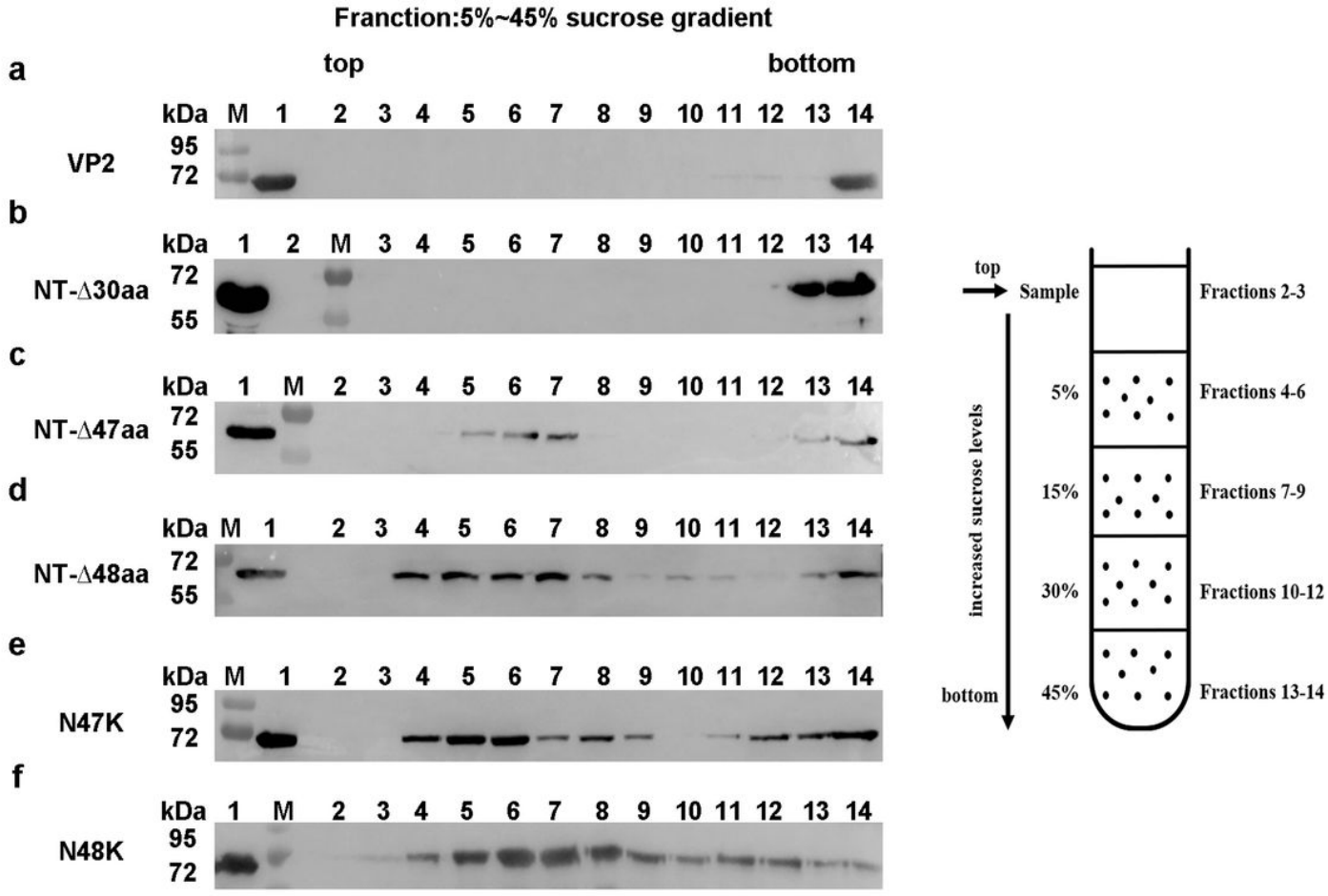

Figure 8

Sucrose gradients results of VP2 and mutant VP2 proteins. Supernatants of E. coli cells expressing VP2 or mutant VP2 proteins were sedimented by 40% saturated ammonium sulfate, dialyzed, and then separated through sucrose gradients. Figures are representative of western blotting analysis of fractions from different sucrose gradients. M, Marker; 1, sedimented sample; 2–3, fractions from sample layer; 4–6, fractions from 5% sucrose layer; 7–9, fractions from 15% sucrose layer; 10–12, fractions from 30% sucrose layer; 13–14, fractions from 45% sucrose layer. a VP2; b NT-Δ30aa; c NT-Δ47aa; d NT-Δ48aa; e N47K; f N48K.

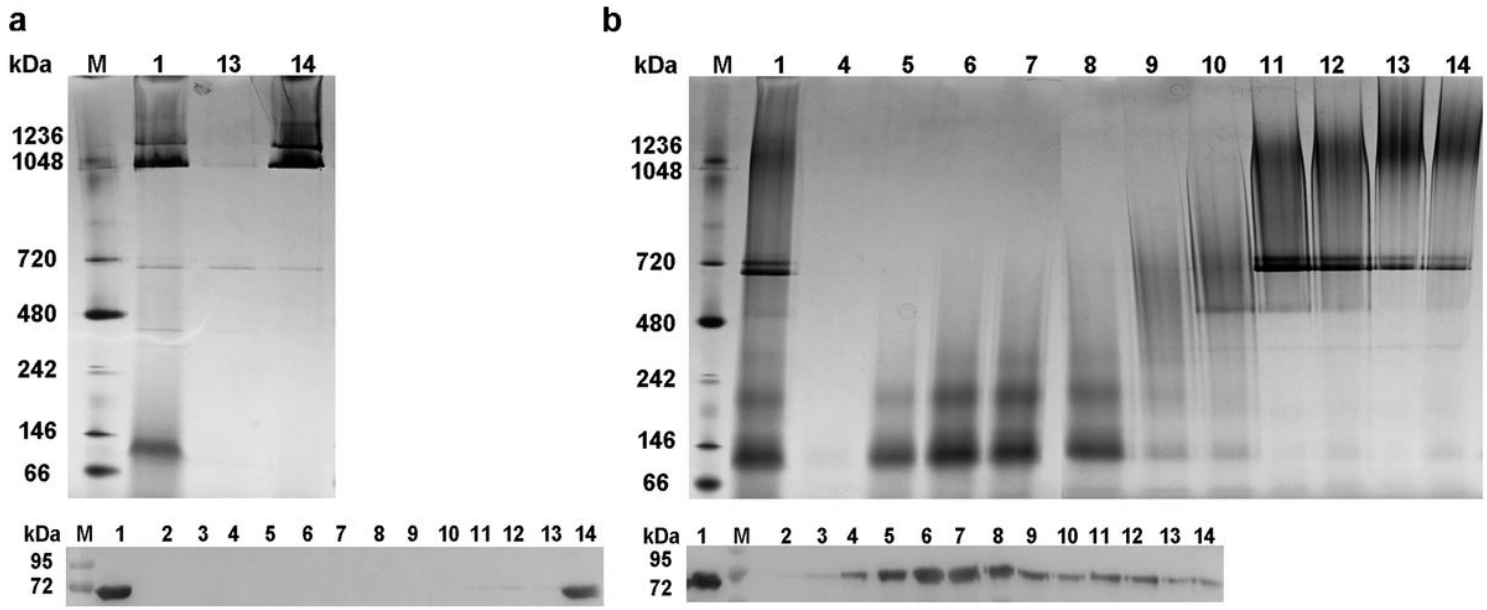

Figure 9

Analysis of the different protein subunits of the VP2 and N48K proteins by Native PAGE. Samples were purified by sucrose gradient sedimentation, and the results were consistent with those shown by western blotting analysis. M, Native Marker; 1, sedimented sample; 2–3, fractions from sample layer; 4–6, fractions from 5% sucrose layer; 7–9, fractions from 15% sucrose layer; 10–12, fractions from 30% sucrose layer; 13–14, fractions from 45% sucrose layer. a VP2; b N48K

Supplementary Files

This is a list of supplementary files associated with this preprint. Click to download.

- Graphicalabstract.tif
- Additionalfiles.docx
- FigureS11.tif
- FigureS12.tif